ACS APPLIED MATERIALS & INTERFACES

Research Article

www.acsami.org

Synthesis of Ultrastable Copper Sulfide Nanoclusters via Trapping the Reaction Intermediate: Potential Anticancer and Antibacterial Applications

Hong-Yin Wang,[†] Xian-Wu Hua,[†] Fu-Gen Wu,*[,†] Bolin Li,[†] Peidang Liu,[†,§] Ning Gu,[†] Zhifei Wang,[⊥] and Zhan Chen*[,‡]

[†]State Key Laboratory of Bioelectronics, School of Biological Science and Medical Engineering, Southeast University, Nanjing 210096, P. R. China

[‡]Department of Chemistry, University of Michigan, 930 North University Avenue, Ann Arbor, Michigan 48109, United States

[§]School of Medicine, Southeast University, Nanjing 210009, P. R. China

[⊥]School of Chemistry and Chemical Engineering, Southeast University, Nanjing 211189, P. R. China

Supporting Information

ABSTRACT: Copper-based nanomaterials have broad applications in electronics, catalysts, solar energy conversion, antibiotics, tissue imaging, and photothermal cancer therapy. However, it is challenging to prepare ultrasmall and ultrastable CuS nanoclusters (NCs) at room temperature. In this article, a simple method to synthesize water-soluble, monodispersed CuS NCs is reported based on the strategy of trapping the reaction intermediate using thiol-terminated, alkyl-containing short-chain poly(ethylene glycol)s (HS-$(CH_2)_{11}$-$(OCH_2CH_2)_6$-OH, abbreviated as MUH). The MUH-coated CuS NCs have superior stability in solutions with varied pH values and are stable in pure water for at least 10 months. The as-prepared CuS NCs were highly toxic to A549 cancer cells at a concentration of higher than 100 μM (9.6 μg/mL), making them be potentially applicable as anticancer drugs via intravenous administration by liposomal encapsulation or by direct intratumoral injection. Besides, for the first time, CuS NCs were used for antibacterial application, and 800 μM (76.8 μg/mL) CuS NCs could completely kill the *E. coli* cells through damaging the cell walls. Moreover, the NCs synthesized here have strong near-infrared (NIR) absorption and can be used as a candidate reagent for photothermal therapy and photoacoustic imaging. The method of trapping the reaction intermediate for simple and controlled synthesis of nanoclusters is generally applicable and can be widely used to synthesize many metal-based (such as Pt, Pd, Au, and Ag) nanoclusters and nanocrystals.

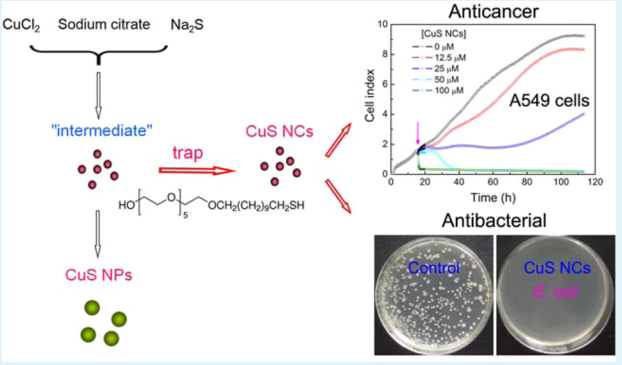

KEYWORDS: *copper sulfide nanocluster, reaction intermediate, ultrastable, antibacterial, short-chain PEG*

1. INTRODUCTION

Copper-based nanomaterials have been developed for applications as printed electronics,[1,2] photovoltaic semiconductors,[3] and antimicrobial products[4,5] due to their lower cost compared to that of other widely used metal nanomaterials such as gold and silver. Among them, copper sulfides (CuS) have attracted a great deal of interest not only due to their unique optical and electrical properties such as photocatalytic,[6,7] photovoltaic,[8,9] plasmonic,[10−14] thermoelectric,[15] ion-storage,[16,17] superionic,[18] and supercapacitor behaviors[19] but also due to their potential broad applications in solar energy conversion,[20] chemical sensing,[21] batteries,[22] and beyond. Besides the traditional semiconductor related applications, CuS materials have received attention recently due to their appealing applications in the field of biomedical engineering, especially for photothermal cancer therapy, bioimaging, and biomolecule detection. For example, using the near-infrared (NIR) absorption property of CuS, various CuS nanomaterials such as hollow CuS nanoparticles (NPs) coated with chitosan, CuS NPs coated with poly(ethylene glycol) (PEG), and PEG-graphene oxide (GO)/CuS nanocomposites were synthesized for photothermal therapy, which can be used in combination with immunotherapy, chemotherapy, as well as simultaneous micropositron emission tomography (PET)/computed tomography (CT) imaging.[23−25] Also, CuS nanomaterials have been used for deep tissue imaging,[26] hydrogen peroxide detection,[27] and photoacoustic visualization of protease activity in vivo.[28] In terms of early diagnosis of cancer, a fluorescent immunosensor

Received: June 16, 2014
Accepted: March 18, 2015
Published: March 18, 2015

DOI: 10.1021/acsami.5b01214
ACS Appl. Mater. Interfaces 2015, 7, 7082−7092

utilizing the oxidation property of CuS NPs was developed for the sensitive detection of human prostate cancer biomarker, prostate specific antigen (PSA).[29]

To utilize these CuS nanomaterials, excellent synthetic control over their crystallization processes is crucial. Generally, the synthetic routes to obtain CuS compounds are diverse and complicated. Moreover, CuS materials can have different phases including Cu_2S (chalcocite),[30] CuS (covellite),[13] and also a variety of nonstoichiometric phases such as $Cu_{1.75}S$ (anilite),[31] $Cu_{1.8}S$ (digenite),[13] and $Cu_{1.97}S$ (djurleite).[13,32] To date, different CuS materials have been prepared by using varied Cu/S ratios,[33] starting materials,[34] stabilizing ligands,[35] and reducing abilities of solvents.[36] However, most of the CuS materials were obtained under air-free conditions[37] or at high temperatures.[38,39] We aim to develop a simple method to synthesize CuS nanomaterials at room temperature. A previous finding reported that during the CuS formation, there were aqueous CuS clusters existing as the intermediates prior to the formation of the final precipitation phase.[40] Interestingly, it was reported that in the preparation process of CuS NPs, a yellow solution could be obtained immediately upon the addition of sodium sulfide and the final product solution changed to green after heating the yellow solution to 90 °C for 15 min.[25] We believe that this yellow solution must be the reaction intermediate. Further characterizations and applications of this intermediate would be possible if an appropriate stabilizing reagent could be introduced to trap and stabilize this intermediate. Besides, the stability of a nanoparticle dispersion is crucial since it determines the property and application of the nanoparticles (e.g., determines how the nanoparticles interact with living organisms).[41] Thus, finding a trapping reagent for stabilizing the CuS nanomaterials in the yellow solution is very important for their environmental or biological uses.

Here, we introduced a thiol-terminated, alkyl-containing short-chain poly(ethylene glycol) ($HS\text{-}(CH_2)_{11}\text{-}(OCH_2CH_2)_6\text{-}OH$, abbreviated as MUH) to trap the CuS nanocluster (NC) intermediate at room temperature (Scheme 1). Characterization of this intermediate demonstrated that monodispersed CuS NCs were obtained with a uniform size of ~5 nm, and these MUH-coated CuS NCs exhibited superior stability in aqueous solution compared to that of other thiol-terminated trapping molecules. High resolution transmission electron microscopy (HRTEM) and X-ray diffraction (XRD) results showed that the phase of the trapped CuS NCs was different from previously reported copper sulfides, indicating the formation of a new phase. Moreover, the CuS NCs synthesized in this research can strongly absorb NIR light, enabling them to be potentially used for photothermal therapy and photoacoustic imaging in the future. Importantly, we have demonstrated that these CuS NCs are highly toxic and can be used as potential anticancer drugs or for antibacterial applications.

2. EXPERIMENTAL SECTION

Materials. Copper(II) chloride ($CuCl_2{\cdot}2H_2O$), sodium sulfide ($Na_2S{\cdot}9H_2O$), dithiothreitol (DTT), and sodium citrate dihydrate were purchased from Aladdin Reagent Company (Shanghai, China). L-Cysteine (Cys), mercaptosuccinic acid (MSA), mercaptoacetic acid (MAA), (11-mercaptoundecyl) hexa-(ethylene glycol) ($HS\text{-}(CH_2)_{11}\text{-}(OCH_2CH_2)_6\text{-}OH$, MUH), and sodium 3-mercapto-1-propanesulfonate ($HS\text{-}(CH_2)_3\text{-}SO_3^-Na^+$, MPS) were ordered from Sigma-Aldrich (St. Louis, MO). 1-Thio-β-D-glucose sodium salt (NaS-Glu) was obtained from Santa Cruz Biotechnology, Inc. Methoxyl PEG thiol (HS-PEG2K) was purchased from Nanocs Inc. Propidium iodide (PI) was purchased from Fanbo Biochemicals Co. Ltd. (Beijing, China). All of the chemicals were directly used without further purification. Dialysis membranes (Spectra/Por6 Dialysis membranes, Regenerated Cellulose, MWCO 3.5K and 10K) were purchased from Spectrumlabs. Deionized water (18.2 MΩ·cm) was obtained from a Milli-Q synthesis system (Millipore, Billerica, MA). A549 human lung cancer cells were obtained from Cell Resource Center of Shanghai Institute for Biological Sciences (Chinese Academy of Sciences, Shanghai, China). AT II human lung normal cells were obtained from Medical School of Southeast University. *E. coli* and *S. aureus* bacteria were obtained from China Center of Industrial Culture Collection (CICC, Beijing, China).

Scheme 1. Schematics of the Formation of CuS NCs[a]

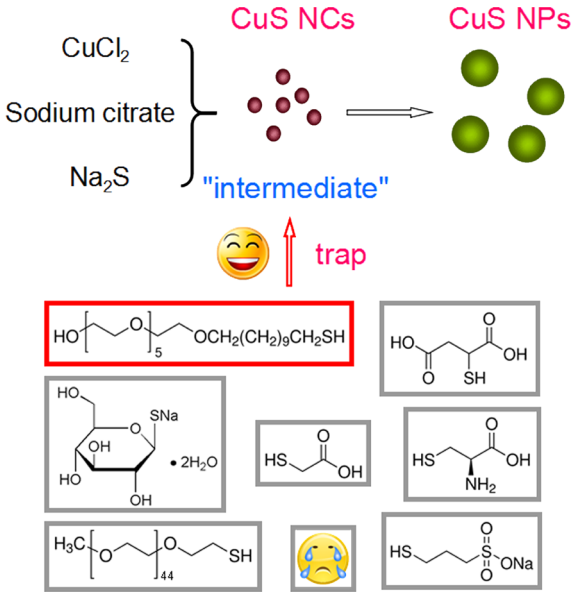

[a]Different kinds of thiol molecules were introduced into the intermediate solutions. Only MUH could trap the intermediate, resulting in the formation of ultrastable CuS NCs.

Synthesis of Copper Sulfide Nanostructures. CuS NP (0.1 mg/mL) were prepared according to a previously reported method.[28] In brief, 17.8 mg of $CuCl_2{\cdot}2H_2O$ and 22.8 mg of sodium citrate dihydrate were dissolved in 100 mL of deionized water upon stirring at room temperature for 5 min. Then, 24.0 mg of $Na_2S{\cdot}9H_2O$ was added to the solution after which the original pale-blue solution changed color and turned to yellow immediately. The yellow solution was directly allowed to react overnight until a green solution was obtained, which indicates the formation of CuS NPs. To improve the stability of the CuS NPs in aqueous solution, for 1 mL of the CuS NPs solution, 2 mg of HS-PEG2K was added, and the mixed solution was incubated for 12 h under stirring at room temperature. Then, the modified CuS NPs were dialyzed (MWCO: 10K) against water for 3 days before final use.

To synthesize CuS NCs, after the formation of the above yellow solution, 46.9 mg of MUH (equal amount in mole to the copper element in the solution) was added to stabilize the reaction intermediate. After shaking at room temperature for 12 h, the obtained CuS NCs were dialyzed (MWCO: 3.5K) for 3 days to remove the reaction residues and unbound ligands. To evaluate the stabilizing effect of MUH, other thiol-containing reagents instead of MUH with the same concentration were also introduced to the yellow solution using the same procedure. Concentrations of CuS NPs and CuS NCs were determined using atomic absorption spectroscopy (AAS, Hitachi 180/80, Japan).

Characterization of CuS Nanostructures. The shape, size, and crystal structure of the CuS nanostructures were investigated by transmission electron microscopy (TEM), high resolution transmission electron microscopy (HRTEM), energy dispersive X-ray spectroscopy (EDS), and X-ray diffraction (XRD). For HRTEM and

DOI: 10.1021/acsami.5b01214
ACS Appl. Mater. Interfaces 2015, 7, 7082−7092

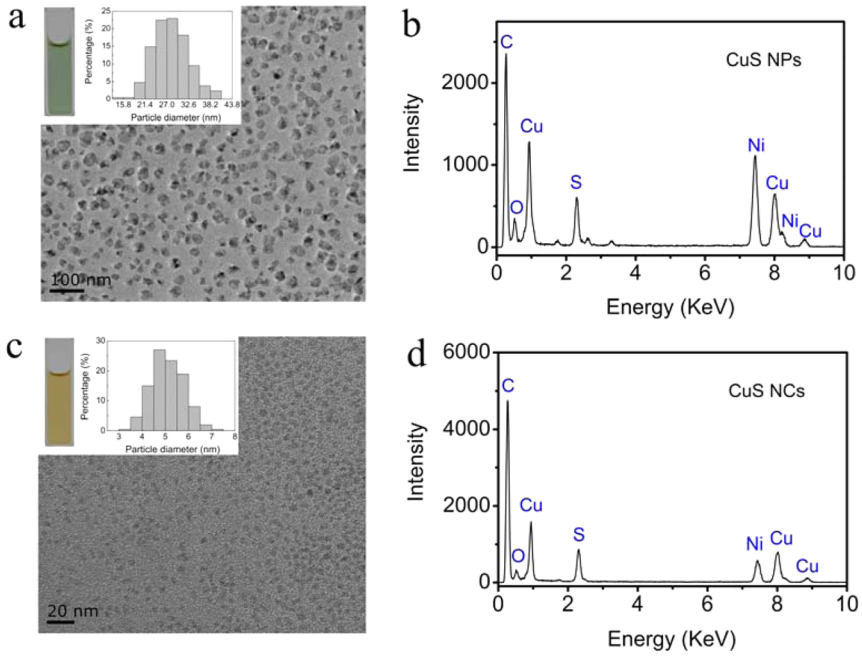

Figure 1. TEM images (left) and EDS results (right) of the CuS NPs (a,b) and CuS NCs (c,d). The concentration of both the green and the yellow solutions in the insets of a and c is 0.1 mg/mL.

EDS, aqueous solutions of CuS nanostructures were dropped on carbon-enhanced copper-free nickle grids. The samples were air-dried and then examined using a transmission electron microscope (FEI TECNAI, G2 20, USA) at an accelerating voltage of 200 kV. XRD was performed using an X-ray diffraction system (BRUKER D8-discover, Germany). UV−vis spectra of CuS nanostructures were recorded on a UV−vis spectrometer (SHIMADZU UV-3150, Japan).

Stability of the MUH-Coated CuS NCs. Stability of the CuS NCs in different pH solutions and in the presence of two small thiol-molecules (DTT and cysteine) were investigated by monitoring the changes of hydrodynamic diameter using a Zetasizer instrument (Nano ZS, Malvern Instruments, UK). Successful conjugation of MUH molecules on CuS NCs was confirmed using a Fourier transform infrared (FTIR) spectrometer (Nicolet iS50, Thermo Scientific, USA).

Cell Culture and Cytotoxicity Evaluation. A549 lung cancer cells and AT II lung normal cells were used to evaluate the cytotoxicity of CuS NCs, CuS NPs, copper ions, and MUH molecules. The two types of cells were both cultured in Dulbecco's modified Eagle's medium (DMEM), supplemented with 10% fetal bovine serum (FBS), and 100 IU/mL penicillin−streptomycin at 37 °C in a humid atmosphere with 5% CO_2. The viability of the treated cells was measured through the MTT (3-[4,5-dimethyl-thiazol-2-yl]-2,5-diphenyltetrazolium bromide) assay. The cells were seeded onto a 96-well plate at a density of 5×10^3 cells per well in 100 μL of complete culture medium. After culturing for 1 day when the cells grew to 80% confluence, the medium in each well was replaced with 100 μL of fresh medium containing a certain concentration of one of the materials mentioned above for testing and further cultured for 24 h. Then the medium containing the tested material was replaced with 100 μL of fresh medium, and 10 μL of MTT solution (5 mg/mL in PBS) was added into each well after which the cells were incubated for an additional 4 h at 37 °C, and the the medium was carefully aspirated. The cells were solubilized in 150 μL of DMSO, and then absorbance at 492 nm was measured against a background control using a microplate reader (Multiskan FC, Thermo-scientific).

Real-Time Analysis of Cell Proliferation. Real-time monitoring of cell growth and proliferation was performed on an impedance-based cell analyzer, the iCELLigence System (ACEA Biosciences Inc.) The growth of the cells leads to an increase of impedance value, shown by an increased cell index value. Differently, inhibition of the cell proliferation or cell death caused by dosed materials can decrease the cell index value. A549 cells were seeded into an E-plate L8 (8 wells) at a density of 1.5×10^4 cells per well in 450 μL of culture medium and allowed to grow for 16 h until the cell index reached ~1.8. Subsequently, different materials such as CuS NCs, CuS NPs, copper ions, and MUH molecules were added into the culture medium, and the data were collected every 15 min for 4 days.

Quantification of Cellular Uptake of Nanomaterials Using ICP-AES. To measure the cellular uptake of CuS NCs and CuS NPs, inductively coupled plasma atomic emission spectroscopy (ICP-AES) experiments were carried out. A549 cells were seeded at a density of 3×10^5 cells per well of a 6-well plate and cultured for 12 h. Then the culture medium was replaced with fresh medium containing 50 μM of CuS NCs or CuS NPs and incubated for 7 h. After washing with PBS three times, the cells were detached using trypsin, collected by centrifugation, counted, and treated with nitric acid at 120 °C for 2 h. Then, the samples were resuspended with 2 mL of deionized water containing 5% hydrochloric acid, and the copper content in each sample was determined by ICP-AES.

Bacterial Culture. *Escherichia coli* (*E. coli*) and *Staphylococcus aureus* (*S. aureus*) were used for the evaluation of the antibacterial ability of CuS NCs. Bacterial cells were cultured in lysogeny broth (LB) medium (5 g/L yeast extract, 10 g/L tryptone, and 0.5 g/L NaCl) under shaking for 12 h at 37 °C until a preliminary bacterial suspension was obtained. Then, the bacterial cells were brought into log phase by reinoculating the bacterial suspension 1:50 into fresh media and grown in a shaking incubator for 2−3 h at 37 °C until an optical density at 600 nm (OD_{600}) of 0.5−0.6 was reached.

Evaluation of Antibacterial Activity. To test the antibacterial activity of CuS NCs, free Cu^{2+} (from $CuCl_2$ solutions) and MUH molecules were used for comparison. Log phase bacterial cells were inoculated 1:10 into 150 μL of fresh LB medium containing different materials for testing and seeded into each well of the 96-well plate and cultured under shaking for 66 h at 37 °C. During the culture process, the optical density at 600 nm of each well was monitored at different time intervals. To eliminate the influence of nanomaterials on the optical density while testing CuS NCs, a well with the LB medium containing the same amount of CuS NCs but no bacterial cells was tested as a control experiment.

The number of the viable bacterial cells in the above wells after a 48 h incubation was analyzed using colony forming unit (CFU) counting.

DOI: 10.1021/acsami.5b01214
ACS Appl. Mater. Interfaces 2015, 7, 7082−7092

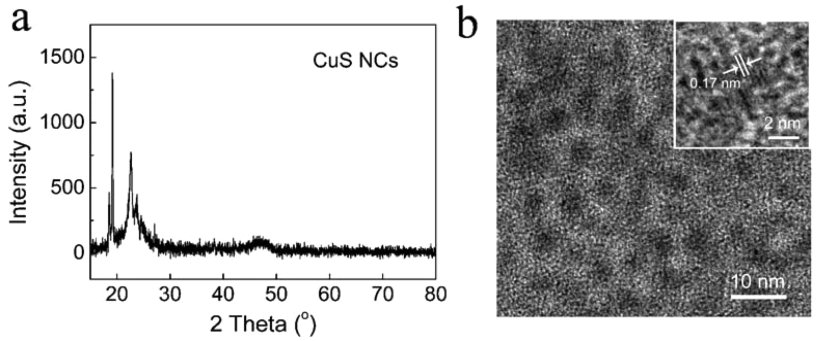

Figure 2. (a) XRD spectrum of the CuS NCs. (b) HRTEM image of the CuS NCs. The inset is an enlarged figure showing one lattice of the sample.

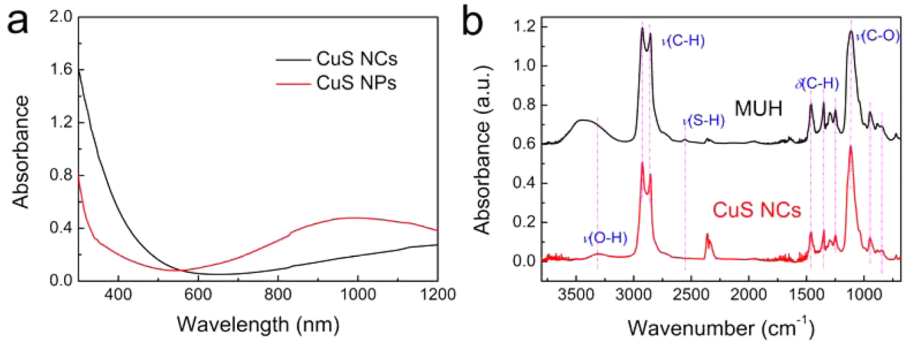

Figure 3. (a) UV−vis spectra of CuS nanostructures (0.1 mg/mL). (b) FTIR spectra of MUH molecules and MUH-coated CuS NCs.

In brief, each culture in the 96-well plate with a dilution factor of 10^4 was plated in triplicate on LB agar plates and incubated at 37 °C for 12 h, and the bacterial colonies formed were counted and recorded.

Morphological Characterization of Bacteria. Morphological changes of the bacteria were characterized by the scanning electron microscope (SEM). Bacteria incubated with different materials for 48 h were collected by centrifugation at 8000 rpm for 3 min and fixed with 2.5% glutaraldehyde overnight at 4 °C. After washing with PBS three times, the bacterial cells were dehydrated through sequential treatment of 30%, 50%, 70%, 80%, 90%, 95%, and 100% ethanol for 15 min and imaged using a scanning electron microscope (SEM, ULTRA Plus, Zeiss, Germany).

Cell Wall/Membrane Integrity Assay. After incubation with different materials for 48 h, bacteria were collected by centrifugation at 8000 rpm for 3 min and stained with propidium iodide (PI, 30 μM) for 15 min in the dark, and then imaged using a confocal microscope (TCS SP8, Leica, Germany).

3. RESULTS AND DISCUSSION

Preparation of CuS Nanostructures. For the synthesis of CuS NPs, a yellow solution was initially formed immediately after mixing $CuCl_2$, sodium citrate, and Na_2S together. This yellow color turned to the final green color upon further reaction at room temperature within 12 h. Interestingly, if this yellow solution was incubated at a lower temperature (e.g., ∼4 °C), the color remained unchanged for at least 2 days, indicating that the lower temperature delayed the formation of the final NPs. On the basis of these observations, we believe that the characteristic yellow color of the CuS solution may represent the existence of a reaction intermediate during the formation of the final CuS NPs.

The intermediate is not stable at room temperature, which seriously limits its potential applications. Thus, finding an efficient way to stabilize the reaction intermediate is crucial. In this work, we successfully trapped the reaction intermediate by introducing a thiol-terminated reagent (MUH) to the yellow solution and found that the trapped intermediate materials are small clusters with an average diameter of ∼5 nm (revealed by TEM in Figure 1c), which we call CuS NCs.

Characterization of CuS Nanostructures. Figure 1a shows the TEM images of the final CuS NPs (without trapping the intermediate) and the appearance of the final green solution (in the inset). The NPs are well-dispersed with an average diameter of approximately 30 nm. In contrast, the CuS NCs (trapped intermediate) have a much smaller size of ∼5 nm with a uniform size distribution (Figure 1c), and the solution is yellow (shown in the inset). EDS results shown in Figure 1b and d confirm the presence of Cu and S elements in both the CuS NPs and CuS NCs.

XRD experiments were carried out to identify the phases of CuS NPs and CuS NCs. The CuS NPs were determined to be the covellite-phase of copper sulfide since the XRD pattern (Figure S1, Supporting Information) is in good agreement with the reported diffraction peaks.[25] For CuS NCs, Figure 2a reveals that there are three main XRD peaks ranging from 10° to 90°. Unexpectedly, it does not match the standard diffraction pattern of any copper sulfides in the database of the international center for diffraction data (ICDD). However, HRTEM results shown in Figure 2b further confirm the crystal structure of the CuS NCs, although the crystal lattice is not clear enough for detailed analysis, and the intensity of the selected area electron diffraction (SAED) pattern (shown in Figure S2, Supporting Information) is also not high. On the basis of these observations, we believe that in the trapping process, the MUH reagents coated on the surface of CuS NCs could form a carbon element/compound wrapping layer, which can disturb the crystallization of the copper sulfides, leading to the formation of crystal precursor structures with a low crystallinity. This speculation is supported by evidence that the absorption of surfactants onto the crystal precursors can occupy

DOI: 10.1021/acsami.5b01214
ACS Appl. Mater. Interfaces 2015, 7, 7082−7092

the surface states and subsequently disturb or prevent further growth of copper sulfide nanoparticles.[42,43] Similar phenomenon can also be observed in palladium nanocrystals.[44] Therefore, a new XRD spectrum of copper sulfide which has not been reported before was obtained, and there is no standard CuS diffraction pattern that can match our XRD result.

The near-infrared (NIR) absorption is an important feature of CuS nanomaterials. The UV−vis spectrum of CuS NCs shown in Figure 3a demonstrates that they can also absorb NIR light (>800 nm), similar to the CuS NPs which have an absorption peak at ∼1000 nm. A previous report showed that CuS NCs of ∼3 nm have maximum NIR absorption at 900 nm.[45] Here, the absorption of our synthesized CuS NCs (5 nm) is broad with a peak above 1200 nm. Also, the absorption of the prepared CuS NCs is weaker than that of CuS NPs (30 nm) below 1200 nm. We believe that the variation in the peak position and intensity of the NIR absorption is caused by the different crystallinities of the two kinds of CuS nanomaterials, and this can be supported by a previous finding showing that the property of the plasmon absorption is related to the phase of the copper sulfides.[13] Nevertheless, the NIR absorption property enables CuS NCs to be potentially useful for photothermal therapy and photoacoustic imaging in the future.

The successful conjugation of MUH molecules on CuS NCs was confirmed by FTIR results. Figure 3b reveals that the characteristic peaks of MUH molecules can be observed in the spectrum of CuS NCs, indicating that the MUH molecules were successfully coated on CuS NCs, leading to the good solubility and excellent stability of the NCs. Moreover, the peak at 2550 cm^{-1} assigned to the SH stretching mode appears in the original MUH spectrum but is absent in the spectrum collected from CuS NCs, further confirming the successful modification of CuS NCs by MUH.

Stability of the MUH-Coated CuS NCs. The stability of the MUH-coated CuS NCs was investigated. As shown in Figure 4a, the picture of the "MUH" sample was taken immediately after dialysis, and the picture of the "MUH-2" sample was taken 10 months after dialysis. They do not show any difference in appearance. The stability of the dialyzed CuS NCs has also been examined by TEM. The results (Figure S3, Supporting Information) show that the sample obtained immediately after dialysis has the same size and shape as those obtained 10 months after dialysis.

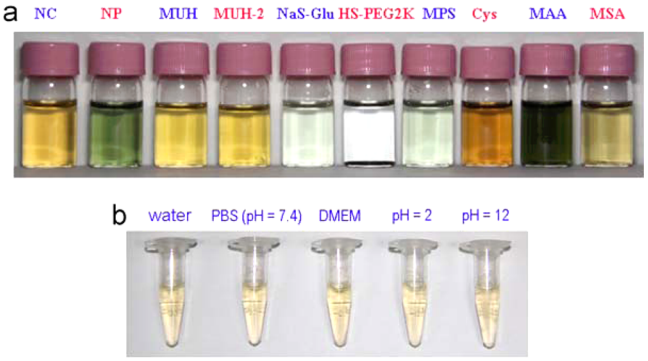

Figure 4. (a) Photographs of CuS solutions (0.1 mg/mL) stabilized by different thiol-containing ligands. "NC" is the freshly prepared CuS NC by mixing $CuCl_2$, sodium citrate, and Na_2S. "NP" is the CuS NP formed by further incubation of a "NC" sample at room temperature for 12 h. "MUH" is the MUH stabilized CuS NCs after dialysis. "MUH-2" is a dialyzed "MUH" sample after storage at room temperature for 10 months. (b) Photos of MUH stabilized CuS NCs (0.1 mg/mL) in pure water, PBS buffer (pH 7.4), complete DMEM cell culture medium supplemented with 10% FBS (phenol red-free), pH 2, and pH 12 solutions. The solutions with pH values of 2 and 12 were prepared by the addition of HCl and NaOH solutions, respectively.

To further investigate if the MUH-coated CuS NCs are stable in various solutions, photographs of the CuS NCs (0.1 mg/mL) in pure water, PBS buffer (pH 7.4), complete DMEM cell culture medium, solutions of pH 2, and pH 12 were taken (Figure 4b). The solutions with pH values of 2 and 12 were prepared by the addition of HCl and NaOH solutions, respectively. The CuS NCs in all of the solutions show the same yellow color, and the solutions are all clear without the formation of any precipitates, indicating that the CuS NCs are stable in cell culture medium as well as in acid and basic solution conditions, making them applicable to various systems. To better understand the stability of CuS NCs in solutions with varied pH values, hydrodynamic diameter in different pH solutions (pH 2, 7, and 12) were measured. As shown in Figure 5a, the diameter of the NCs remains unchanged at around 5−6 nm at tested pH values, exhibiting the superb stability. Such superior stability of the MUH-coated CuS NCs can benefit many future applications of these materials.

Besides MUH, several other thiol-terminated stabilizing reagents were also investigated to trap the reaction intermediate. At first, the commonly used PEG derivative, HS-PEG2K, was studied. As shown in Figure 4a, adding HS-PEG2K to the yellow solution produced precipitation after several hours. Therefore, the use of this material to trap CuS NCs was not successful. Besides, glucose (Glu) was also tested since it has been frequently used to coat nanoparticles to improve their biocompatibility and increase the cellular uptake efficiency of these nanoparticles.[46−48] After the addition of NaS-Glu to the yellow solution, the color gradually changed from yellow to light green after a few days at room temperature (Figure 4a), implying that NaS-Glu also cannot prevent the conversion of CuS NCs to CuS NPs. Although cysteine (Cys) could initially stabilize the formed NCs and the yellow color of the solution did not change, several days after dialysis, some precipitates were observed at the bottom of the vial. In addition, other small thiol molecules such as sodium 3-mercapto-1-propanesulfonate (MPS), mercaptoacetic acid (MAA), and mercaptosuccinic acid (MSA) also failed to trap the CuS NCs to prevent the formation of the final large CuS NPs (Figure 4a).

The above experiments demonstrated the critical role the MUH molecule played for the successful preparation of the ultraclean and ultrastable CuS NCs. The MUH molecule contains three segments: the mercapto group (−SH), the methylene group (C_{11}), and the short-chain polyethylene glycols (EG_6). All these components are important for preparing and stabilizing the CuS NCs. The mercapto group is to bind to copper atoms through the Cu−S bond,[49,50] while the alkyl chain (C_{11}) serves as a hydrophobic shield to stabilize nanoclusters and prevent other thiol-containing molecules from replacing the bound thiol-ligands.[51] In a previous research, it was found that if the Au NPs were first coated with HS-PEG2K or HS-PEG5K, which does not have this hydrophobic shield, some small thiol-terminated molecules (such as cysteine) can replace the surface HS-PEGs, causing the possible instability of the NPs.[51] Herein, the stability of CuS NCs in the presence of

DOI: 10.1021/acsami.5b01214
ACS Appl. Mater. Interfaces 2015, 7, 7082−7092

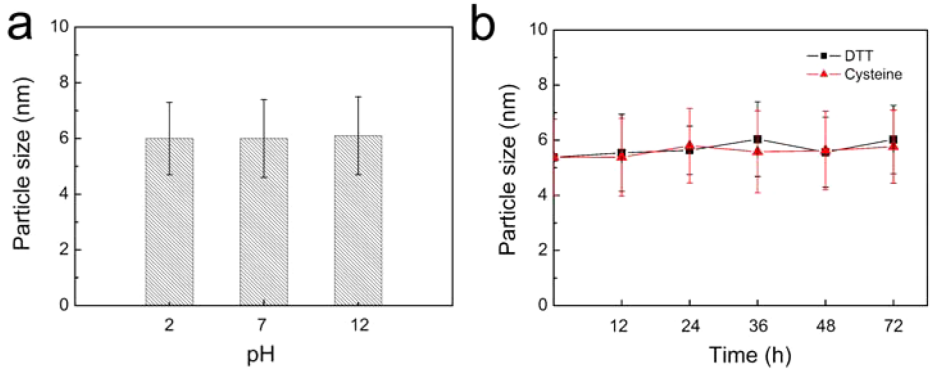

Figure 5. (a) Hydrodynamic diameter changes of CuS NCs at different pH values revealed by dynamic light scatting (DLS). The different pH values were adjusted by the addition of HCl or NaOH solutions. (b) Hydrodynamic diameter changes of CuS NCs in the presence of DTT (50 mM) or cysteine (200 μM) as a function of time.

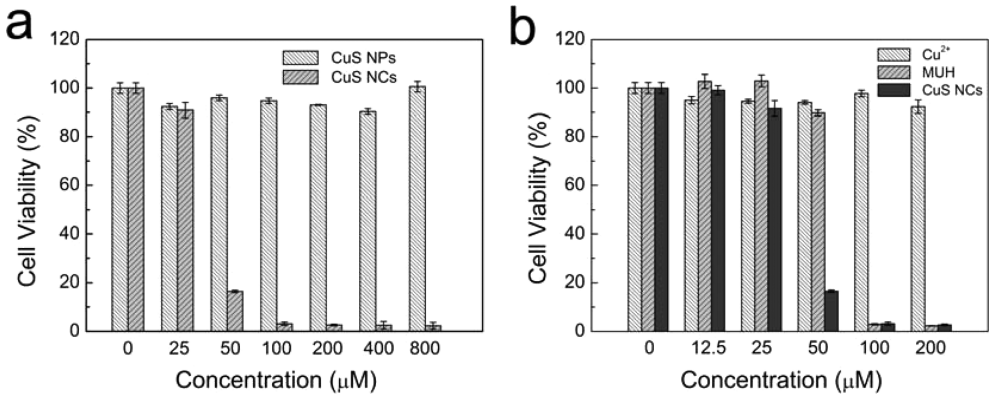

Figure 6. Cytotoxicity of different materials to A549 cancer cells (24 h) tested by the MTT assay. (a) Comparison of CuS NCs with CuS NPs. (b) Comparison of CuS NCs with copper ions and MUH molecules.

two thiol-terminated molecules, dithiothreitol (DTT) and cysteine, was also investigated by monitoring the hydrodynamic diameter of the NCs. Similar to a previous work,[51] DTT (50 mM) was selected as a positive control because of its high efficiency for causing ligand displacement, while cysteine (200 μM) was chosen due to its presence in DMEM culture medium and in real blood. As shown in Figure 5b, the diameter of the CuS NCs remained unchanged at 5−6 nm in the presence of DTT or cysteine after an incubation time of 72 h, indicating that the MUH molecules on the surface of CuS NCs effectively inhibited the replacement by other thiol-terminated small molecules, confirming the stability of the as-prepared CuS NCs. Finally, the hydrophilic EG_n part on MUH is also important. It can increase the water solubility and also endow the CuS NCs with a superb capability of preventing nonspecific adsorption of proteins[52−54] and can therefore "mask" the CuS NCs from the host's immune system (reduced immunogenicity and antigenicity) in many future applications.

Cytotoxicity of CuS NCs and CuS NPs. To evaluate the cytotoxicity of CuS nanostructures in vitro, A549 cancer cells were used as a model cell line. MTT assay results demonstrated that the CuS NPs were almost nontoxic to A549 cells even after exposure to the highest concentration of 800 μM (CuS 76.8 μg/mL) for 24 h (Figure 6a). This low cytotoxicity of the CuS NPs endows them with many potential applications in biomedical fields, such as photoacoustic imaging probes[28] and photothermal therapy.[45] In contrast, the CuS NCs obtained by trapping reaction intermediate were highly toxic to the cells. When 50 μM (4.8 μg/mL) of CuS NCs was dosed, the cell viability decreased to around 15%, and when exposed to a higher concentration (above 100 μM), all of the cancer cells were killed. The much higher cytotoxicity of CuS NCs may be related to their higher cellular uptake efficiency due to their smaller size as compared with those of the CuS NPs. After incubation of 50 μM CuS NCs (and 50 μM of CuS NPs) with A549 cells for 7 h, ICP-AES results (Figure S4, Supporting Information) reveal that for CuS NCs, the copper content in A549 cells was 0.33 ng per 1000 cells, while for CuS NPs, the amount was 0.23 ng per 1000 cells. Although the cellular uptake of CuS NCs is higher than that of CuS NPs, the detailed mechanism for the much higher cytotoxicity of CuS NCs still needs further investigation.

To this end, the toxicities of copper ions, MUH molecules, and CuS NCs against A549 cancer cells were evaluated via the MTT assay (Figure 6b). Under the tested conditions, copper ions were not toxic (cell viability was above 94%), suggesting that the observed cytotoxicity of CuS NCs was not caused by the release of copper ions. For MUH, it was toxic and all the cells were killed when its concentration was above 100 μM. However, CuS NCs were the most toxic sample in particular compared with the MUH molecules at the same concentration of 50 μM (the viability of the CuS NCs-treated cells was below 20%, while that of the MUH-treated cells was ~90%). Notably, in the CuS NC synthesis process, the MUH molecules used for trapping the CuS NCs were dosed with the equal mole amount of the Cu element. However, the amount of MUH molecules on the CuS NCs (with the diameter of 5 nm) was estimated to be less than 1/5 of the dosage (see Supporting Information).

DOI: 10.1021/acsami.5b01214
ACS Appl. Mater. Interfaces 2015, 7, 7082−7092

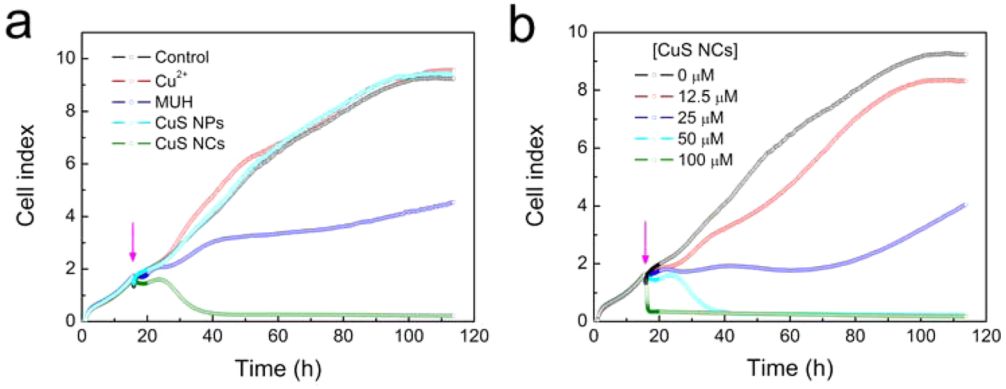

Figure 7. Real-time analysis of the proliferation process of A549 lung cancer cells after the introduction of various materials. Pink arrows indicate the material introduction time point. (a) Effect of different materials (with the same concentration of 50 μM) on the cell index. The materials tested include CuS NCs, CuS NPs, copper ions, and MUH molecules. (b) Effect of CuS NC concentration on the cell index.

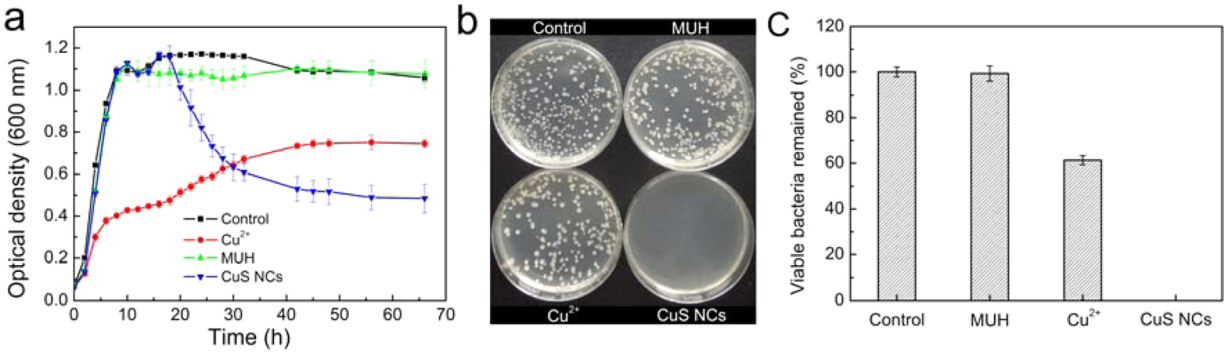

Figure 8. (a) Optical density of *E. coli* suspensions measured at 600 nm after exposure to CuS NCs (800 μM), copper ions (800 μM), and MUH solutions (400 μM) for 66 h. (b) Bacteria colonies formed on LB-agar plates. The cells were seeded from the 48 h incubation samples. (c) Number of viable bacteria remaining in the 48 h incubation samples. Data were counted from the CFU results in b.

Therefore, this evidence further demonstrates that the CuS NCs are far more toxic than the MUH molecules. This might be due to the high local concentration of MUH on CuS NCs which can more effectively interact with and enter the cells. Then perhaps many factors such as the surface defects of the nanomaterials may play a synergistic role in the cytotoxicity of CuS NCs in addition to the CuS compounds and MUH ligands.

Besides the MTT assay, real-time cell analysis (RTCA) experiments were also carried out to monitor the growth of A549 cells for 4 days after the introduction of different materials. Consistent with the MTT results, Figure 7a demonstrates that at the concentration of 50 μM, CuS NPs and copper ions did not have influence on cell proliferation, and the cell growth curves were almost the same as that of the untreated control group, confirming that they are not toxic at this concentration. For MUH molecules, the growth of cells was significantly inhibited and the cell index dropped to around half the value of the control group, implying their moderate cytotoxicity. In contrast, after adding 50 μM of CuS NCs, the cell index decreased gradually, and almost all of the cells were killed after 24 h. In addition, the cytotoxicity of CuS NCs was found to be concentration-dependent (Figure 7b). When lower concentrations of CuS NCs were dosed, the growth of A549 cells was significantly (at 25 μM) or slightly (at 12.5 μM) inhibited. Notably, after dosing with 100 μM (9.6 μg/mL) CuS NCs, acute cell death was observed within 15 min, and the cell index sharply dropped to 0.4 within 1 h, implying that almost all of the cells were killed. Such acute toxicity makes CuS NCs have the potential to be developed as anticancer drugs. However, the MTT assay reveals that they were also highly toxic to AT II normal lung cells (Figure S5, Supporting Information). Thus, to avoid the damage to normal cells, these highly toxic CuS NCs can be used for direct intratumoral injection or intravenous administration after liposomal encapsulation. The in vivo application of these CuS NCs as anticancer drugs is currently under investigation.

Antibacterial Activity of CuS NCs. Infection by pathogenic bacteria is a major disease that threatens human health. Besides the widely used traditional antibiotics, several new antimicrobial materials have been developed such as functional polymers,[55−57] graphene or graphene-based nanocomposites,[58,59] and metal-based (especially silver) nanoparticles.[60,61] However, in terms of copper-based antibacterial materials, although copper sulfate solution,[62] metallic copper,[63] and copper nanoparticles[5,64] have demonstrated the antibacterial properties, this is the first time to demonstrate that CuS NCs can be used as a potential antimicrobial reagent. To investigate the bactericidal effect, we have compared the antibacterial ability of CuS NCs with that of free Cu^{2+} ions and MUH molecules against *E. coli*. Because of a good correlation between the turbidity of the bacterial suspension and the amounts of the bacteria, the microplate assay was adopted for measuring the antibacterial activity of CuS NCs. Results shown in Figure 8a reveal that for the first 18 h, growth of CuS NC (800 μM, or 76.8 μg/mL)-treated *E. coli* is almost the same as that of the control group. However, after that, the OD_{600} starts to decline until it reaches ~0.5 and maintains at this value

DOI: 10.1021/acsami.5b01214
ACS Appl. Mater. Interfaces 2015, 7, 7082−7092

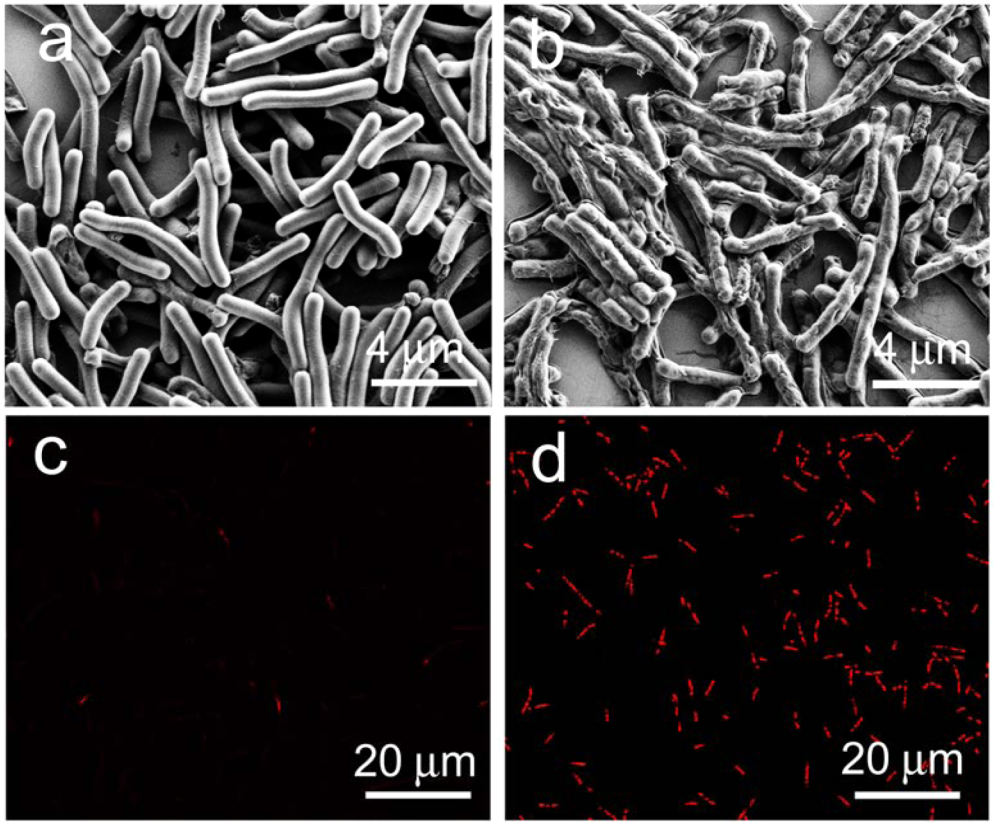

Figure 9. Characterizations of *E. coli* after incubation with CuS NCs (800 μM) for 48 h. Panels a and b are SEM images of control cells and drug-treated cells, respectively. Panels c and d are confocal fluorescence images of the PI stained control cells and CuS NC-treated cells, respectively.

thereafter, indicating that the antibacterial activity of CuS NCs was activated after 18 h. In contrast, the MUH solution shows no antibacterial activity at 400 μM. Note that the MUH concentration of 400 μM is already much higher than that on the surface of CuS NCs (160 μM, as estimated to be 1/5 of the Cu element). However, a higher concentration of MUH (800 μM) could inhibit bacterial growth at the first 10 h, after which the cells grew rapidly to the log phase (Figure S6, Supporting Information). The antibacterial activity of MUH may be attributed to the hydrophobic segment of the MUH ligand since the hydrophobic chain can insert into bacterial cell membrane and induce bactericidal effects.[65] Besides, the highly reactive hydroxyl group at the terminal of MUH may also have the potential to damage the bacterial cells. For copper ions, their antibacterial property is already known, and we have shown in this work that 800 μM copper ions slightly inhibited the growth of *E. coli* with the OD_{600} value decreasing to below 0.8.

Besides the OD_{600} monitoring assay, the number of viable bacterial cells after 48 h of treatment was measured using the CFU counting method (Figure 8b and c). The number of viable cells in the MUH-treated group is almost the same as that in the control group, in good agreement with the OD_{600} result (Figure 8a). For copper ions, 61% of the cells were still alive, confirming its bacterial inhibition effect. Interestingly, although the CuS NC-treated cells have the OD_{600} value of ~0.5 after 48 h of treatment, there was no colony formed on the LB agar plate, implying that almost all of the cells were dead. Thus, the OD_{600} value of ~0.5 is due to the growth of bacterial cells during the initial growth period (from 0 to 18 h), after which the cells were gradually killed during the time period of 18 to 40 h. The minimum concentration we have tested for the antibacterial experiment is 400 μM. However, such a small concentration of CuS NCs does not have a significant antibacterial effect, and thus, we only show the result of a higher concentration (800 μM) and conclude that the minimum inhibition concentration (MIC) is 800 μM (76.8 μg/mL).

To further investigate the antibacterial mechanism of CuS NCs, morphological changes of *E. coli* were studied via SEM (Figure 9). After incubation with 800 μM CuS NCs for 48 h, the cell walls are wrinkled and damaged (Figure 9b), in contrast to that of the untreated cells which are smooth and intact (Figure 9a). In addition, the integrity of the cell walls was also examined by a fluorescent nucleic acid dye (PI) which can only stain the DNA of the dead cells by penetrating through the damaged membranes.[66] Compared with the rarely stained untreated cells (Figure 9c), almost all the CuS NC-treated *E. coli* cells were stained by PI (Figure 9d), confirming the death of the cells and the break of the cell walls. These results reveal that the antibacterial activity of CuS NCs was achieved by damaging the cell walls of the bacteria, making the CuS NCs be powerful to fight against drug resistance of bacteria since it is hard for bacteria to develop resistance to membrane-disrupting antibiotics.[67] Likely, the MUH molecules on CuS NC surfaces having a high local concentration can interact with the cell walls effectively and damage the cell walls to kill the bacteria. At the same time, some copper ions may be released from the CuS NCs, enhancing the antimicrobial activity.

In addition to the Gram-negative *E. coli* cells, the Gram-positive *S. aureus* bacteria were also chosen to evaluate the antibacterial ability of CuS NCs via monitoring OD_{600} under

DOI: 10.1021/acsami.5b01214
ACS Appl. Mater. Interfaces 2015, 7, 7082−7092

the same experimental conditions. Unfortunately, after treatment for 48 h, there is almost no antibacterial effect on *S. aureus* cells, and only a little growth inhibition effect can be observed (Figure S7, Supporting Information), suggesting that CuS NCs can selectively induce the cell death of Gram-negative *E. coli* but not the Gram-positive *S. aureus*. This may be due to the different structures and chemical compositions of their cell walls.[68] The presence of a thick peptidoglycan layer in the cell walls of Gram-positive bacteria may provide bacteria with better protection against the CuS NCs.[69]

4. CONCLUSIONS

In this research, we developed a simple method to synthesize CuS NCs at room temperature by trapping the reaction intermediate using MUH. MUH also served as a protecting ligand to stabilize CuS NCs. The synthesized CuS NCs are extremely stable, monodispersed, uniformly distributed in size, and can absorb NIR light (for photothermal therapy and photoacoustic imaging). It was demonstrated that the CuS NCs were highly toxic to A549 cancer cells at a concentration >100 μM (9.6 μg/mL), making them potential anticancer drugs via intravenous administration by liposomal encapsulation or by direct intratumoral injection. Besides, for the first time, CuS NCs were used as antibacterial reagents, and 800 μM (76.8 μg/mL) CuS NCs could completely kill *E. coli* cells via damaging their cell walls. The method of trapping the reaction intermediate developed here is simple and generally applicable for synthesizing other metal-based (such as Pt, Pd, Au, and Ag) nanocrystals.

■ ASSOCIATED CONTENT

Supporting Information

Additional XRD spectrum, SEAD pattern, TEM, ICP-AES results, MTT assay results, OD_{600} for *E. coli* and *S. aureus*, and the estimation of the MUH density on the CuS NC surface. This material is available free of charge via the Internet at http://pubs.acs.org.

■ AUTHOR INFORMATION

Corresponding Authors

*(F.-G.W.) E-mail: wufg@seu.edu.cn.
*(Z.C.) E-mail: zhanc@umich.edu.

Notes

The authors declare no competing financial interest.

■ ACKNOWLEDGMENTS

This work was supported by grants from the National Key Basic Research Program of China (973 Program) (No. 2013CB933904), the Natural Science Foundation of China (21303017), the Fundamental Research Funds for the Central Universities (2242014K10010), the Scientific Research Foundation of Graduate School of Southeast University (YBJJ1412), and Graduate Students' Scientific Research Innovation Project of Jiangsu Province Ordinary University (No.CXZZ13 0122). Z.C. thanks University of Michigan for the support of his sabbatical.

■ REFERENCES

(1) Lee, Y.; Choi, J.; Lee, K. J.; Stott, N. E.; Kim, D. Large-Scale Synthesis of Copper Nanoparticles by Chemically Controlled Reduction for Applications of Inkjet-Printed Electronics. *Nanotechnology* **2008**, *19*, 415604/1−415604/7.

(2) Riha, S. C.; Johnson, D. C.; Prieto, A. L. Cu_2Se Nanoparticles with Tunable Electronic Properties Due to a Controlled Solid-State Phase Transition Driven by Copper Oxidation and Cationic Conduction. *J. Am. Chem. Soc.* **2011**, *133*, 1383−1390.

(3) Wu, Y.; Wadia, C.; Ma, W. L.; Sadtler, B.; Alivisatos, A. P. Synthesis and Photovoltaic Application of Copper(I) Sulfide Nanocrystals. *Nano Lett.* **2008**, *8*, 2551−2555.

(4) Ren, G. G.; Hu, D. W.; Cheng, E. W. C.; Vargas-Reus, M. A.; Reip, P.; Allaker, R. P. Characterisation of Copper Oxide Nanoparticles for Antimicrobial Applications. *Int. J. Antimicrob. Agents* **2009**, *33*, 587−590.

(5) Ingle, A. P.; Duran, N.; Rai, M. Bioactivity, Mechanism of Aciton, and Cytotoxicity of Copper-Based Nanoparticles: A Review. *Appl. Microbiol. Biotechnol.* **2014**, *98*, 1001−1009.

(6) Ratanatawanate, C.; Bui, A.; Vu, K.; Balkus, K. J., Jr. Low-Temperature Synthesis of Copper(II) Sulfide Quantum Dot Decorated TiO_2 Nanotubes and Their Photocatalytic Properties. *J. Phys. Chem. C* **2011**, *115*, 6175−6180.

(7) Cheng, Z. G.; Wang, S. Z.; Wang, Q.; Geng, B. Y. A Facile Solution Chemical Route to Self-assembly of CuS Ball-Flowers and Their Application as an Efficient Photocatalyst. *CrystEngComm* **2010**, *12*, 144−149.

(8) Xu, Q.; Huang, B.; Zhao, Y. F.; Yan, Y. F.; Noufi, R.; Wei, S. H. Crystal and Electronic Structures of Cu_xS Solar Cell Absorbers. *Appl. Phys. Lett.* **2012**, *100*, 061906/1−061906/4.

(9) Lee, H.; Yoon, S. W.; Kim, E. J.; Park, J. In-Situ Growth of Copper Sulfide Nanocrystals on Multiwalled Carbon Nanotubes and Their Application as Novel Solar Cell and Amperometric Glucose Sensor Materials. *Nano Lett.* **2007**, *7*, 778−784.

(10) Kriegel, I.; Rodríguez-Fernández, J.; Da Como, E.; Lutich, A. A.; Szeifert, J. M.; Feldmann, J. Tuning the Light Absorption of $Cu_{1.97}S$ Nanocrystals in Supercrystal Structures. *Chem. Mater.* **2011**, *23*, 1830−1834.

(11) Luther, J. M.; Jain, P. K.; Ewers, T.; Alivisatos, A. P. Localized Surface Plasmon Resonances Arising from Free Carriers in Doped Quantum Dots. *Nat. Mater.* **2011**, *10*, 361−366.

(12) Zhao, Y. X.; Burda, C. Development of Plasmonic Semiconductor Nanomaterials with Copper Chalcogenides for a Future with Sustainable Energy Materials. *Energy Environ. Sci.* **2012**, *5*, 5564−5576.

(13) Zhao, Y. X.; Pan, H. C.; Lou, Y. B.; Qiu, X. F.; Zhu, J. J.; Burda, C. Plasmonic $Cu_{2-x}S$ Nanocrystals: Optical and Structural Properties of Copper-Deficient Copper(I) Sulfides. *J. Am. Chem. Soc.* **2009**, *131*, 4253−4261.

(14) Kanehara, M.; Arakawa, H.; Honda, T.; Saruyama, M.; Teranishi, T. Large-Scale Synthesis of High-Quality Metal Sulfide Semiconductor Quantum Dots with Tunable Surface-Plasmon Resonance Frequencies. *Chem.—Eur. J.* **2012**, *18*, 9230−9238.

(15) Ge, Z. H.; Zhang, B. P.; Chen, Y. X.; Yu, Z. X.; Liu, Y.; Li, J. F. Synthesis and Transport Property of $Cu_{1.8}S$ as a Promising Thermoelectric Compound. *Chem. Commun.* **2011**, *47*, 12697−12699.

(16) Cai, R.; Chen, J.; Zhu, J. X.; Xu, C.; Zhang, W. Y.; Zhang, C. M.; Shi, W. H.; Tan, H. T.; Yang, D.; Hng, H. H.; Lim, T. M.; Yan, Q. Y. Synthesis of Cu_xS/Cu Nanotubes and Their Lithium Storage Properties. *J. Phys. Chem. C* **2012**, *116*, 12468−12474.

(17) Dilena, E.; Dorfs, D.; George, C.; Miszta, K.; Povia, M.; Genovese, A.; Casu, A.; Pratoa, M.; Manna, L. Colloidal $Cu_{2-x}(S_ySe_{1-y})$ Alloy Nanocrystals with Controllable Crystal Phase: Synthesis, Plasmonic Properties, Cation Exchange and Electrochemical Lithiation. *J. Mater. Chem.* **2012**, *22*, 13023−13031.

(18) Miller, T. A.; Wittenberg, J. S.; Wen, H.; Connor, S.; Cui, Y.; Lindenberg, A. M. The Mechanism of Ultrafast Structural Switching in Superionic Copper(I) Sulphide Nanocrystals. *Nat. Commun.* **2013**, *4*, 1369/1−1369/7.

(19) Zhu, T.; Xia, B. Y.; Zhou, L.; Lou, X. W. Arrays of Ultrafine CuS Nanoneedles Supported on a CNT Backbone for Application in Supercapacitors. *J. Mater. Chem.* **2012**, *22*, 7851−7855.

(20) Lin, M. C.; Lee, M. W. $Cu_{2-x}S$ Quantum Dot-Sensitized Solar Cells. *Electrochem. Commun.* **2011**, *13*, 1376−1378.

DOI: 10.1021/acsami.5b01214
ACS Appl. Mater. Interfaces 2015, 7, 7082−7092

(21) Šetkus, A.; Galdikas, A.; Mironas, A.; Šimkiene, I.; Ancutiene, I.; Janickis, V.; Kačiulis, S.; Mattogno, G.; Ingo, G. M. Properties of Cu_xS Thin Film Based Structures: Influence on the Sensitivity to Ammonia at Room Temperatures. *Thin Solid Films* **2001**, *391*, 275−281.
(22) Lai, C. H.; Huang, K. W.; Cheng, J. H.; Lee, C. Y.; Hwang, B. J.; Chen, L. J. Direct Growth of High-Rate Capability and High Capacity Copper Sulfide Nanowire Array Cathodes for Lithium-Ion Batteries. *J. Mater. Chem.* **2010**, *20*, 6638−6645.
(23) Guo, L. R.; Yan, D. D.; Yang, D. F.; Li, Y. J.; Wang, X. D.; Zalewski, O.; Yan, B. F.; Lu, W. Combinatorial Photothermal and Immuno Cancer Therapy Using Chitosan-Coated Hollow Copper Sulfide Nanoparticles. *ACS Nano* **2014**, *8*, 5670−5681.
(24) Bai, J.; Liu, Y. W.; Jiang, X. E. Multifunctional PEG-GO/CuS Nanocomposites for Near-Infrared Chemo-Photothermal Therapy. *Biomaterials* **2014**, *35*, 5805−5813.
(25) Zhou, M.; Zhang, R.; Huang, M.; Lu, W.; Song, S. L.; Melancon, M. P.; Tian, M.; Liang, D.; Li, C. A Chelator-Free Multifunctional [^{64}Cu]CuS Nanoparticle Platform for Simultaneous Micro-PET/CT Imaging and Photothermal Ablation Therapy. *J. Am. Chem. Soc.* **2010**, *132*, 15351−15358.
(26) Ku, G.; Zhou, M.; Song, S. L.; Huang, Q.; Hazle, J.; Li, C. Copper Sulfide Nanoparticles As a New Class of Photoacoustic Contrast Agent for Deep Tissue Imaging at 1064 nm. *ACS Nano* **2012**, *6*, 7489−7496.
(27) Bo, X. J.; Bai, J.; Wang, L. X.; Guo, L. P. In Situ Growth of Copper Sulfide Nanoparticles on Ordered Mesoporous Carbon and Their Application as Nonenzymatic Amperometric Sensor of Hydrogen Peroxide. *Talanta* **2010**, *81*, 339−345.
(28) Yang, K.; Zhu, L.; Nie, L. M.; Sun, X. L.; Cheng, L.; Wu, C. X.; Niu, G.; Chen, X. Y.; Liu, Z. Visualization of Protease Activity In Vivo Using an Activatable Photo-Acoustic Imaging Probe Based on CuS Nanoparticles. *Theranostics* **2014**, *4*, 134−141.
(29) Zhu, Y. D.; Peng, J.; Jiang, L. P.; Zhu, J. J. Fluorescent Immunosensor Based on CuS Nanoparticles for Sensitive Detection of Cancer Biomarker. *Analyst* **2014**, *139*, 649−655.
(30) Rivest, J. B.; Fong, L. K.; Jain, P. K.; Toney, M. F.; Alivisatos, A. P. Size Dependence of a Temperature-Induced Solid−Solid Phase Transition in Copper(I) Sulfide. *J. Phys. Chem. Lett.* **2011**, *2*, 2402−2406.
(31) Liufu, S. C.; Chen, L. D.; Yao, Q.; Huang, F. Q. In Situ Assembly of Cu_xS Quantum-Dots into Thin Film: A Highly Conductive P-Type Transparent Film. *J. Phys. Chem. C* **2008**, *112*, 12085−12088.
(32) Lotfipour, M.; Machani, T.; Rossi, D. P.; Plass, K. E. α-Chalcocite Nanoparticle Synthesis and Stability. *Chem. Mater.* **2011**, *23*, 3032−3038.
(33) Ghezelbash, A.; Korgel, B. A. Nickel Sulfide and Copper Sulfide Nanocrystal Synthesis and Polymorphism. *Langmuir* **2005**, *21*, 9451−9456.
(34) Kumar, P.; Gusain, M.; Nagarajan, R. Synthesis of $Cu_{1.8}S$ and CuS from Copper-Thiourea Containing Precursors; Anionic (Cl^-, NO_3^-, SO_4^{2-}) Influence on the Product Stoichiometry. *Inorg. Chem.* **2011**, *50*, 3065−3070.
(35) Lim, W. P.; Wong, C. T.; Ang, S. L.; Low, H. Y.; Chin, W. S. Phase-Selective Synthesis of Copper Sulfide Nanocrystals. *Chem. Mater.* **2006**, *18*, 6170−6177.
(36) Freymeyer, N. J.; Cunningham, P. D.; Jones, E. C.; Golden, B. J.; Wiltrout, A. M.; Plass, K. E. Influence of Solvent Reducing Ability on Copper Sulfide Crystal Phase. *Cryst. Growth Des.* **2013**, *13*, 4059−4065.
(37) Xie, Y.; Riedinger, A.; Prato, M.; Casu, A.; Genovese, A.; Guardia, P.; Sottini, S.; Sangregorio, C.; Miszta, K.; Ghosh, S.; Pellegrino, T.; Manna, L. Copper Sulfide Nanocrystals with Tunable Composition by Reduction of Covellite Nanocrystals with Cu^+ Ions. *J. Am. Chem. Soc.* **2013**, *135*, 17630−17637.
(38) Bryks, W.; Wette, M.; Velez, N.; Hsu, S. W.; Tao, A. R. Supramolecular Precursors for the Synthesis of Anisotropic Cu_2S Nanocrystals. *J. Am. Chem. Soc.* **2014**, *136*, 6175−6178.
(39) Nørby, P.; Johnsen, S.; Iversen, B. B. In Situ X-ray Diffraction Study of the Formation, Growth, and Phase Transition of Colloidal $Cu_{2-x}S$ Nanocrystals. *ACS Nano* **2014**, *8*, 4295−4303.
(40) Luther, G. W., III; Theberge, S. M.; Rozan, T. F.; Rickard, D.; Rowlands, C. C.; Oldroyd, A. Aqueous Copper Sulfide Clusters as Intermediates during Copper Sulfide Formation. *Environ. Sci. Technol.* **2002**, *36*, 394−402.
(41) Labille, J.; Jonathan Brant, J. Stability of Nanoparticles in Water. *Nanomedicine* **2010**, *5*, 985−998.
(42) Kore, R. H.; Kulkarni, J. S.; Haram, S. K. Effect of Nonionic Surfactants on the Kinetics of Disproportion of Copper Sulfide Nanoparticles in the Aqueous Sols. *Chem. Mater.* **2001**, *13*, 1789−1793.
(43) Wu, C. Y.; Zhou, G. F.; Mao, D.; Zhang, Z. H.; Wu, Y. L.; Wang, W. J.; Luo, L. B.; Wang, L.; Yu, Y. Q.; Hu, J. G.; Zhu, Z. F.; Zhang, Y.; Jie, J. S. CTAB Assisted Synthesis of CuS Microcrystals: Synthesis, Mechanism, and Electrical Properties. *J. Mater. Sci. Technol.* **2013**, *29*, 1047−1052.
(44) Liu, Y.; Wang, C.; Wei, Y. J.; Zhu, L. Y.; Li, D. G.; Jiang, J. S.; Markovic, N. M.; Stamenkovic, V. R.; Sun, S. H. Surfactant-Induced Postsynthetic Modulation of Pd Nanoparticle Crystallinity. *Nano Lett.* **2011**, *11*, 1614−1617.
(45) Li, Y. B.; Lu, W.; Huang, Q.; Li, C.; Chen, W. Copper Sulfide Nanoparticles for Photothermal Ablation of Tumor Cells. *Nanomedicine* **2010**, *5*, 1161−1171.
(46) Tsuji, T.; Kuwamura, N.; Yoshinari, N.; Konno, T. Synthesis and Coordination Behavior of a Bipyridine Platinum(II) Complex with Thioglucose. *Inorg. Chem.* **2013**, *52*, 5350−5358.
(47) Roa, W.; Xiong, Y. P.; Chen, J.; Yang, X. Y.; Song, K.; Yang, X. H.; Kong, B. H.; Wilson, J.; Xing, J. Z. Pharmacokinetic and Toxicological Evaluation of Multi-functional Thiol-6-fluoro-6-deoxy-d-glucose Gold Nanoparticles in Vivo. *Nanotechnology* **2012**, *23*, 375101/1−375101/10.
(48) Connor, E. E.; Mwamuka, J.; Gole, A.; Murphy, C. J.; Wyatt, M. D. Gold Nanoparticles Are Taken up by Human Cells but Do Not Cause Acute Cytotoxicity. *Small* **2005**, *1*, 325−327.
(49) Howard-Lock, H. E. Structures of Gold(I) and Silver(I) Thiolate Complexes of Medicinal Interest: A Review and Recent Results. *Met.-Based Drugs* **1999**, *6*, 201−209.
(50) Kacprzak, K. A.; Lopez-Acevedo, O.; Häkkinen, H.; Grönbeck, H. Theoretical Characterization of Cyclic Thiolated Copper, Silver, and Gold Clusters. *J. Phys. Chem. C* **2010**, *114*, 13571−13576.
(51) Larson, T. A.; Joshi, P. P.; Sokolov, K. Preventing Protein Adsorption and Macrophage Uptake of Gold Nanoparticles via a Hydrophobic Shield. *ACS Nano* **2012**, *6*, 9182−9190.
(52) Prime, K. L.; Whitesides, G. M. Adsorption of Proteins onto Surfaces Containing End-attached Oligo(ethylene oxide): A Model System Using Self-assembled Monolayers. *J. Am. Chem. Soc.* **1993**, *115*, 10714−10721.
(53) Bergström, K.; Holmberg, K.; Safranj, A.; Hoffman, A. S.; Edgell, M. J.; Kozlowski, A.; Hovanes, B. A.; Harris, J. M. Reduction of Fibrinogen Adsorption on PEG-coated Polystyrene Surfaces. *J. Biomed. Mater. Res.* **1992**, *26*, 779−790.
(54) Harbers, G. M.; Emoto, K.; Greef, C.; Metzger, S. W.; Woodward, H. N.; Mascali, J. J.; Grainger, D. W.; Lochhead, M. J. A Functionalized Poly(ethylene glycol)-Based Bioassay Surface Chemistry that Facilitates Bio-immobilization and Inhibits Non-specific Protein, Bacterial, and Mammalian Cell Adhesion. *Chem. Mater.* **2007**, *19*, 4405−4414.
(55) Yuan, H. X.; Wang, B.; Lv, F. T.; Liu, L. B.; Wang, S. Conjugated-Polymer-Based Energy-Transfer Systems for Antimicrobial and Anticancer Applications. *Adv. Mater.* **2014**, *26*, 6978−6982.
(56) Liu, L. B.; Chen, J.; Wang, S. Flexible Antibacterial Film Deposited with Polythiophene-Porphyrin Composite. *Adv. Healthcare Mater.* **2013**, *2*, 1582−1585.
(57) Chong, H.; Nie, C. Y.; Zhu, C. L.; Yang, Q.; Liu, L. B.; Lv, F. T.; Wang, S. Conjugated Polymer Nanoparticles for Light-Activated Anticancer and Antibacterial Activity with Imaging Capability. *Langmuir* **2012**, *28*, 2091−2098.

DOI: 10.1021/acsami.5b01214
ACS Appl. Mater. Interfaces 2015, 7, 7082−7092

(58) Hu, W. B.; Peng, C.; Luo, W. J.; Lv, M.; Li, X. M.; Li, D.; Huang, Q.; Fan, C. H. Graphene-Based Antibacterial Paper. *ACS Nano* **2010**, *4*, 4317−4323.
(59) Liu, S. B.; Zeng, T. H.; Hofmann, M.; Burcombe, E.; Wei, J.; Jiang, R. R.; Kong, J.; Chen, Y. Antibacterial Activity of Graphite, Graphite Oxide, Graphene Oxide, and Reduced Graphene Oxide: Membrane and Oxidative Stress. *ACS Nano* **2011**, *5*, 6971−6980.
(60) Kim, J. S.; Kuk, E.; Yu, K. N.; Kim, J. H.; Park, S. J.; Lee, H. J.; Kim, S. H.; Park, Y. K.; Park, Y. H.; Hwang, C. Y.; Kim, Y. K.; Lee, Y. S.; Jeong, D. H.; Cho, M. H. Antimicrobial Effects of Silver Nanoparticles. *Nanomed.-Nanotechnol. Biol. Med.* **2007**, *3*, 95−101.
(61) Shrivastava, S.; Bera, T.; Roy, A.; Singh, G.; Ramachandrarao, P.; Dash, D. Characterization of Enhanced Antibacterial Effects of Novel Silver Nanoparticles. *Nanotechnology* **2007**, *18*, 225103/1−225103/9.
(62) Sierra, M.; Sanhueza, A.; Alcántara, R.; Sánchez, G. Antimicrobial Evaluation of Copper Sulfate(II) on Strains of Enterococcus Faecalis. In Vitro Study. *J. Oral Res.* **2013**, *2*, 114−118.
(63) Grass, G.; Rensing, C.; Solioz, M. Metallic Copper as an Antimicrobial Surface. *Appl. Environ. Microbiol.* **2011**, *77*, 1541−1547.
(64) Chatterjee, A. K.; Chakraborty, R.; Basu, T. Mechanism of Antibacterial Activity of Copper Nanoparticles. *Nanotechnology* **2014**, *25*, 135101/1−135101/12.
(65) Yang, D.; Pornpattananangkul, D.; Nakatsuji, T.; Chan, M.; Carson, D.; Huang, C. M.; Zhang, L. F. The Antimicrobial Activity of Liposomal Lauric Acids Against *Propionibacterium acnes*. *Biomaterials* **2009**, *30*, 6035−6040.
(66) Jung, W. K.; Koo, H. C.; Kim, K. W.; Shin, S.; Kim, S. H.; Park, Y. H. Antibacterial Activity and Mechanism of Action of the Silver Ion in *Staphylococcus aureus* and *Escherichia coli*. *Appl. Environ. Microbiol.* **2008**, *74*, 2171−2178.
(67) Chen, H.; Wang, B.; Zhang, J. Y.; Nie, C. Y.; Lv, F. T.; Liu, L. B.; Wang, S. Guanidinium-Pendant Oligofluorene for Rapid and Specific Identification of Antibiotics with Membrane-Disrupting Ability. *Chem. Commun.* **2015**, *51*, 4036−4039.
(68) Yuan, H. X.; Liu, Z.; Liu, L. B.; Lv, F. T.; Wang, Y. L.; Wang, S. Cationic Conjugated Polymers for Discrimination of Microbial Pathogens. *Adv. Mater.* **2014**, *26*, 4333−4338.
(69) Tang, J.; Chen, Q.; Xu, L. G.; Zhang, S.; Feng, L. Z.; Cheng, L.; Xu, H.; Liu, Z.; Peng, R. Graphene Oxide-Silver Nanocomposite as a Highly Effective Antibacterial Agent with Species-Specific Mechanisms. *ACS Appl. Mater. Interfaces* **2013**, *5*, 3867−3874.

DOI: 10.1021/acsami.5b01214
ACS Appl. Mater. Interfaces 2015, 7, 7082−7092